Orbital
The electronic journal of chemistry

the electronic journal of chemistry

Full Paper | http://dx.doi.org/10.17807/orbital.v17i4.16546

Application of Amorphous Alloy $Co_{69}Nb_{25}B_6$ for Orthopedic Implants

Luciano Nascimento [a*], José William de Lima Souza [b], Suédina Maria de Lima Silva [c], and Ana Cristina Figueiredo de Melo Costa [d]

This study investigates the potential of the amorphous alloy $Co_{69}Nb_{25}B_6$ as a promising biomaterial for orthopedic implants. The alloy was produced via high-energy milling (HEM). An amorphous $Co_{69}Nb_{25}B_6$ powdered alloy was prepared by mechanical alloying process. Notably, 20 g of powder were used with a powder-to-ball weight ratio of approximately 20:1 at a rotation speed of 300 rpm. Characterization of the $Co_{69}Nb_{25}B_6$ alloy was carried out using X-ray diffraction (XRD), scanning electron microscopy (SEM), and a vibrating sample magnetometer (VSM). The results showed that the amorphous $Co_{69}Nb_{25}B_6$ alloy powder exhibited a high degree of amorphous phase formation, a flake-like morphology, and a particle size of approximately 10 μm. Additionally, the $Co_{69}Nb_{25}B_6$ alloy demonstrated soft ferromagnetic behavior, with a saturation magnetization of 0.23 emu/g after 20 h of milling. This research highlights the potential of amorphous alloy $Co_{69}Nb_{25}B_6$ as a viable material for traumatic orthopedic medical devices.

Graphical abstract

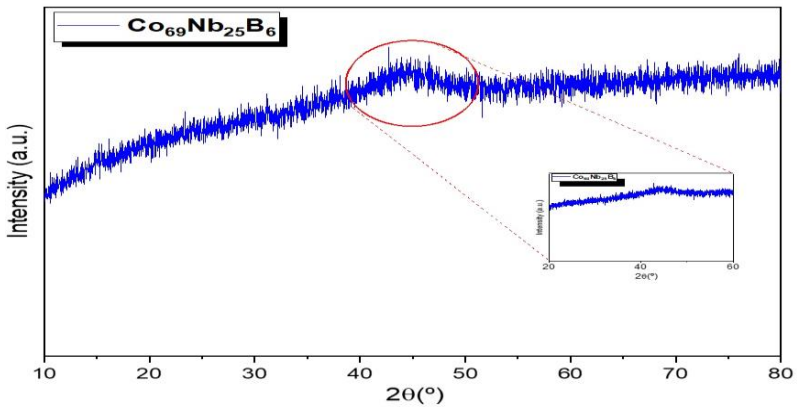

Keywords

Biomaterial
Amorphous Alloy $Co_{69}Nb_{25}B_6$
Traumatic Orthopedic

Article history

Received 22 Aug 2022
Accepted 18 Apr 2025
Available online 05 Jul 2025

Handling Editor: Marcos S. Amaral

1. Introduction

Amorphous alloys, also referred to as metallic glasses, constitute an advanced class of materials characterized by a non-crystalline atomic structure, being one of the most promising classes in biomaterials. They exhibit short-range atomic order but lack long-range translational symmetry, akin to the structural disorder observed in conventional glasses [1]. Despite the apparent atomic-scale disorder and the complexity in characterizing their electronic structure,

[a*,d]Federal University of Campina Grande-UFCG. Academic Unit of Materials Engineering, Laboratory of Synthesis of Ceramic Materials – LabSMaC, Av. Aprígio Veloso, 882 - Bodocongó, CEP: 58429-900, Campina Grande – Paraíba, Brazil. [b,c]Federal University of Campina Grande-UFCG. Academic Unit of Materials Engineering, Laboratory of Evaluation and Development of Biomaterials of the Northeast – CERTBIO, Av. Aprígio Veloso, 882 - Bodocongó, CEP: 58429-900, Campina Grande – Paraíba, Brazil. *Corresponding author. E-mail: **luciano.ufcg@gmail.com**

extensive studies have demonstrated that their non-periodic arrangement follows specific local ordering principles and is not entirely stochastic. In recent decades, they have attracted significant attention for biomedical applications due to their exceptional mechanical properties, superior hardness, excellent tribological and corrosion resistance, and outstanding biocompatibility [2,3]. Various amorphous alloy systems based on elements such as Fe, Co, Nb, Zr, Ni, Ti, and Pt have been synthesized and extensively studied. Among metallic glasses, Co-based amorphous alloys stand out due to their relatively low cost, excellent mechanical properties (such as high strength and hardness), strong glass-forming ability, corrosion resistance, and acceptable biocompatibility [4,5]. These alloys typically exhibit densities between 7.7 and 8.5 g/cm³, with systems like $Co_{70}Fe_2Mn_4Si_{12}B_{10}$ reaching around 7.81 g/cm³. Despite their relatively high elastic modulus (approximately 230 GPa), certain structural characteristics help mitigate stress shielding, thereby promoting more efficient bone regeneration. Moreover, the corrosion behavior of Co-based amorphous alloys contributes positively to osteointegration. In physiological environments, their degradation can lead to the formation of calcium phosphate layers—derived from elements such as Ca, P, and Si—which enhance bone bonding and accelerate the osteosynthesis process. Importantly, the corrosion products are non-toxic, soluble oxides that are naturally excreted through urine. Additionally, alloying cobalt with metalloid elements improves both the mechanical performance and chemical stability of these materials, making them promising candidates for orthopedic and biomedical applications. The amorphous phase is characterized by its ability to exist in a metastable state without crystallizing, allowing it to be obtained at relatively low cooling rates [6]. Consequently, Co-based amorphous alloys are frequently employed as biomedical implant materials, particularly in the field of traumatic orthopedic surgery, where they exhibit satisfactory biocompatibility and low toxicity [7]. However, for such materials to be considered viable as long-term implants, their tolerance to simulated body fluids must be thoroughly evaluated—especially for load-bearing applications such as joint replacement devices in traumatic orthopedics [8].

Several processing techniques have been developed to produce amorphous alloys, including thermal spraying, physical vapor deposition, chemical vapor deposition, melt spinning, and high-energy milling (HEM) [9]. Among these, HEM has demonstrated a strong ability to achieve high consolidation of metal powders. It is a fully solid-state processing technique that is not constrained by phase diagrams and is capable of producing amorphous alloys that cannot be fabricated through conventional rapid solidification methods [10,11]. Moreover, during the subsequent consolidation process, viscous flow from the supercooled liquid region ($\Delta T = T_x - T_g$, where T_x is the onset temperature of crystallization and T_g is the glass transition temperature) can be exploited to fabricate amorphous alloys or bulk metallic glasses (BMGs), thereby overcoming the size limitations associated with rapid solidification techniques [12,13]. To the best of our knowledge, no studies have reported the synthesis of an amorphous alloy of the $Co_{69}Nb_{25}B_6$ composition via high-energy milling, despite its significant potential for use in orthopedic implants. From the perspective of orthopedic applications, the use of this metallic system offers promising prospects, as its mechanical properties could enhance the performance and outcomes of orthopedic surgical procedures across a range of clinical scenarios.

2. Material and Methods

The nominal composition of the amorphous alloy ($Co_{69}Nb_{25}B_6$) was prepared by blending high-purity elemental powders: cobalt (Co, 99.99%, 60 µm), niobium (Nb, 99.99%, 60 µm), and boron (B, 99.9%, 58 µm), sourced from Sigma-Aldrich and Companhia Brasileira de Metalurgia e Mineração (CBMM). The powder mixture was subjected to high-energy milling (HEM) to induce amorphization. Milling was carried out using a Fritsch Pulverisette P5.7 planetary ball mill, equipped with hardened steel vials and 10 mm diameter hardened steel balls. The powder weight was 20 g and the powder-to-ball-weight ratio was about 20:1. The rotation speed was 300 rpm. To prevent cold welding and reduce agglomeration and contamination, toluene (C_7H_8, 2 mL) was employed as a process control agent (PCA), filling approximately one-third of the vial volume to ensure complete immersion of the powders and grinding media, thereby promoting efficient energy transfer. A fully amorphous structure was achieved after 20 h of milling. Structural characterization was performed by X-ray diffraction (XRD) using a Bruker D2 Phaser diffractometer with $CuK_{\alpha 1}$ radiation (λ = 1.54056 Å), operating at 40 kV and 30 mA. Measurements were conducted in the 2θ range of 10–80°, with a step size of 0.016° and a counting time of 5 s per step. The morphology of the $Co_{69}Nb_{25}B_6$ powders was examined via scanning electron microscopy (SEM) using a TESCAN VEGA3 system operating at 30 kV, with an imaging magnification of 5.00 kx. High-field magnetization measurements were performed using a Microsense EZ7 Vibrating Sample Magnetometer (VSM) under magnetic fields up to 2.7 T (21.5 kOe) across a temperature range of 77–1000 K. The magnetic field was applied parallel to the longitudinal axis of the sample to minimize demagnetization effects. The resulting magnetization curves were analyzed using the least squares fitting method. The coercive field (Hc) was determined using a coercimeter equipped with a permalloy probe.

3. Results and Discussion

Figure 1 shows the X-ray diffraction (XRD) pattern of the as-received amorphous $Co_{69}Nb_{25}B_6$ alloy. The broad diffuse halo observed within the red circle confirms the amorphous structure of the material. However, the X-ray diffraction (XRD) pattern (Figure 1), spectrum shows that the as quenched material was typically amorphous. Within a wide 2θ range (30-50º) only a revealed a broad diffuse halo centered at 2θ ≈ 44°, indicating the absence of distinct diffraction peaks associated with crystalline phases, suggesting that the alloy possesses an amorphous structural character [14].

The morphological evolution of the $Co_{69}Nb_{25}B_6$ alloy were investigated by SEM as shown in Figure 2 in the time 20 h of milling fabricated by HEM.

The microstructure reveals irregularly shaped and agglomerated particles with a predominantly flake-like morphology [15]. These lamellar particles exhibit rough surfaces and appear to be formed through repeated cold welding and fracturing mechanisms, which are characteristic of prolonged mechanical alloying. The magnification used was 5.00 kx, and the scale bar corresponds to 10 µm, indicating that most of the particles are in the micrometer range. Owing to severe plastic deformation and welding mechanisms during the milling, the powder mixtures started getting agglomerated. With prolonged milling, the agglomerated clusters became smaller, more rounded and uniform in shape.

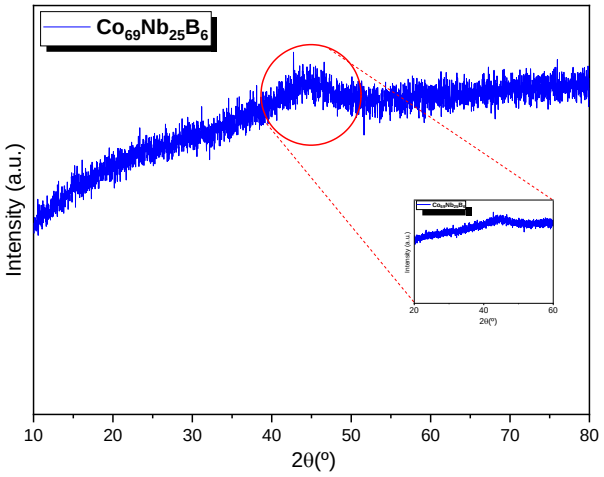

Fig. 1. XRD pattern of the $Co_{69}Nb_{25}B_6$ amorphous alloy milled for 20 h.

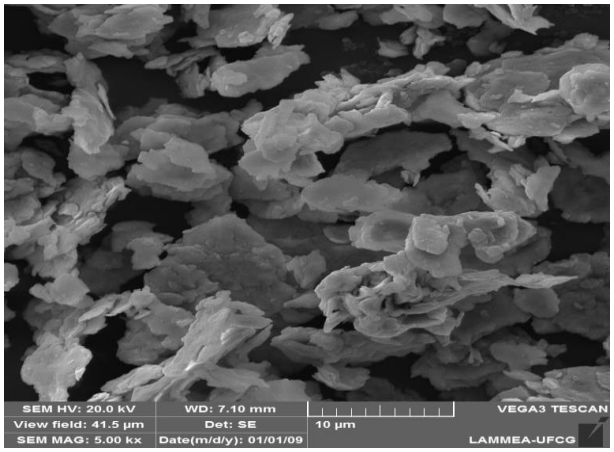

Fig. 2. SEM image of the $Co_{69}Nb_{25}B_6$ powder milled for 20h.

Figure 3 presents the magnetization (M) versus applied magnetic field (H) hysteresis loop for the amorphous alloy $Co_{69}Nb_{25}B_6$, measured at room temperature (T = 300 K).

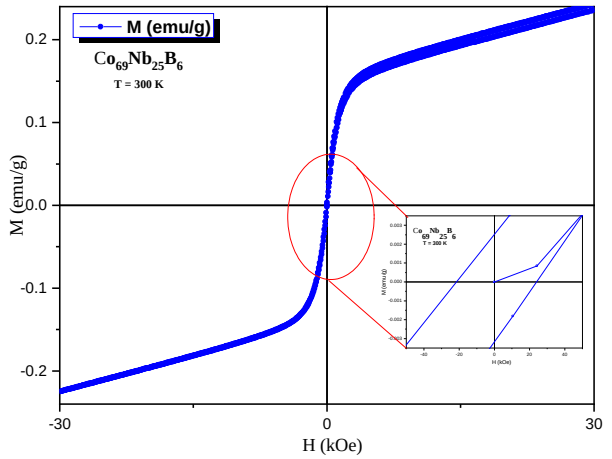

Fig. 3. Magnetization curve of the $Co_{69}Nb_{25}B_6$ amorphous alloy after 20 h of milling.

The curve exhibits typical soft ferromagnetic behavior, with a saturation magnetization (M_s) of approximately 0.23 emu/g and a remanent magnetization (M_r) of about 0.04 emu/g. The coercive field (H_c), as highlighted in the inset, is approximately 2.5 kOe. Typical behavior of soft ferromagnetic materials is observed, evidenced by the low coercivity and small remanent magnetization. The narrow shape of the curve around H=0 indicates that the material can be magnetized and demagnetized with relative ease, a desirable characteristic in applications that require energy efficiency, such as transformer cores and magnetic switching devices. In addition, the magnetization tends to saturate for magnetic fields greater than ±20 kOe, reaching approximately 0.2 emu/g, which demonstrates the ability of the alloy to align its magnetic moments with the applied field. The enlarged insertion of the curve in the central region allows us to observe more precisely the low values of H_c and M_r, reinforcing the character of a magnetically soft material. This behavior is strongly associated with the amorphous nature of the alloy, which, because it does not present a periodic crystalline structure, significantly reduces the magnetocrystalline anisotropy and facilitates the movement of the domain walls, making this alloy system a promising candidate for use in orthopedic implants and other biointegrated technologies.

Although cobalt (Co) is a ferromagnetic material, its magnetic contribution may be reduced when alloyed with elements that exhibit different magnetic behaviors. In the case of the $Co_{69}Nb_{25}B_6$ amorphous alloy, the inclusion of niobium (Nb), a paramagnetic element, and boron (B), which is diamagnetic, likely alters the magnetic response of the system [16]. Such a low Mr/Ms around 0.173 value also suggests the presence of multidomain structures in the powder particles of the alloy. In these structures, magnetization changes can occur primarily via the movement of Bloch domain walls rather than coherent rotation. These processes are characteristic of soft magnetic materials and are particularly influenced by the disordered atomic structure of amorphous alloys, which lacks long-range crystallographic order. An de $Mr/Ms \ll 0.1$, indicates that the powder particles exhibit a multidomain structure, in which magnetization changes may primarily occur through domain wall motion under relatively low magnetic fields [17]. Therefore, the magnetic behavior observed in the $Co_{69}Nb_{25}B_6$ alloy can be strongly attributed to processes occurring in its amorphous volume. In this disordered matrix, the magnetic anisotropy is significantly reduced, allowing for easier domain wall motion. Moreover, the random distribution of uniaxial anisotropic ferromagnetic particles and the lack of grain boundaries contribute to magnetic isotropy on a macroscopic scale [18]. This explains why even in the presence of a high concentration of ferromagnetic Co, the overall magnetic response is softened. It has been suggested that the addition of small fractions of metalloids with high electronegativity, such as B, is beneficial to increase the magnetization (M) between Co and Nb atoms [19]. In this case, the exchange integral is not very sensitive with variation of the Co-Co distance or 3d orbital radius of Co, according to the shape of the Bethe-slater curve [20]. In contrast, the addition of B is expected to slightly decrease the magnetization (M), due to chemical bonding and possible hybridization of orbitals for the B atom with 3d orbitals for Co and Nb atoms [21, 22].

4. Conclusions

- The broad diffuse halo centered around $2\theta \approx 44°$ indicates the lack of sharp diffraction peaks characteristic of crystalline phases, thereby confirming the predominantly amorphous nature of the material.
- SEM analysis reveals a microstructure composed of

particles with irregular and agglomerated morphology, predominantly in the form of flakes, with sizes around 10 μm, formed as a result of the amorphization process present in the $Co_{69}Nb_{25}B_6$ alloy;

- The magnetization process of M_s=0.23 emu/g for a saturation field is very close to 2.5 kOe for an amorphous alloy of the $Co_{69}Nb_{25}B_6$ type, which exhibits a curve typical of soft ferromagnetic behavior;
- Metalloid fractions with high electronegativity in the $Co_{69}Nb_{25}B_6$ alloy, such as boron (B), enhance the saturation magnetization (M_s) by promoting hybridization of B atom orbitals with the 3d orbitals of Co and Nb atoms.
- Owing to its distinct morphological features and structurally disordered atomic arrangement, the amorphous alloy $Co_{69}Nb_{25}B_6$ demonstrates considerable promise for advanced biomedical applications

Acknowledgments

The authors wish to thank CAPES for the financial support of this research, would like to thank the Multidisciplinary Laboratory of Active Materials and Structures (LaMMEA) of UAEM and Magnetic Testing (LESMA) of the Physics Academic Unit (UAF) of the Science and Technology Center of UFCG and CBMM - Companhia Brasileira de Metalurgia e Mineração.

Author Contributions

Luciano Nascimento (Investigation, Conceptualization, Data Curation, Supervision, Vali dation, Writing – First Draft and Final Review); José William de L. Souza Martins (Investigation, Conceptualization, Supervision, Validation, Writing –Original Draft and Editing); Suédina M. de L. Silva (Investigation, Conceptualization, Supervision, Validation, Writing –Original Draft, Writing –Review and Editing); Ana Cristina F. M. Costa (Investigation, Conceptualization, Methodology, Supervision, Validation, Writing –Original Draft, Writing –Review and Editing).

References and Notes

[1] Wang, J.; Ma, Y.; Guo, S.; Jiang, W.; Liu, Q. *Mater. Des.* **2018**, *153*, 308. [Crossref]

[2] Lin, H. C.; Tsai, P. H.; Ke, J. H.; Li, J. B.; Jang, J. S. C.; Huang, C. H.; Haung, J. C. *Intermetallics* **2014**, 55, 22. [Crossref]

[3] Khan, M. M.; Shabib, I.; Haider, W. *Scr. Mater.* **2019**, *162*, 223. [Crossref]

[4] Zhao, J.; Gao, Q.; Wang, H.; Shu, F.; Zhao, H.; He, W.; Yu, Z. *J. Alloys Compd.* **2019**, *785*, 846. [Crossref]

[5] Zhou, Z.; Wei, Q.; Li, Q.; Jiang, B.; Chen, Y.; Sun, Y. *Mater. Sci. Eng. C* **2016**, *69*, 46. [Crossref]

[6] Nascimento, L.; Leal, E.; Guedes, D. G.; Costa, M. R.; Silva, A. L. D.; Guedes, G. G.; Costa, A. C. F. D. M. *Matéria (Rio de Janeiro)* **2024**, 29, e20240228. [Crossref]

[7] Ford, D. C.; Hicks, D.; Oses, C.; Toher, C.; Curtarolo, S. *Acta Mater.* **2019**, *176*, 297. [Crossref]

[8] Li, T. H.; Liao, Y. C.; Song, S. M.; Jiang, Y. L.; Tsai, P. H.; Jang, J. S. C.; Huang, J. C. *Intermetallics* **2018**, *93*, 162. [Crossref]

[9] Xu, Y.; Zhou, S.; Liao, B.; Zhao, S.; Dai, X.; Chen, D. *J. Mater. Res. Technol.* **2019**, *8*, 3929. [Crossref]

[10] Révész, Á.; Kovács, Z. *Materials Transactions* **2019**, *60*, 1283. [Crossref]

[11] Sergiienko, R. A.; Shcheretskyu, O. A.; Zadorozhnyy, V. Y.; Verkhovliuk, A. M.; Louzguine-Luzgin, D. V. *J. Alloys Compd.* **2019**, *791*, 477. [Crossref]

[12] Abrosimova, G. E.; Aronin, A. S. *Crystallogr. Rep.* **2020**, *65*, 573. [Crossref]

[13] Ibrahim, M. Z.; Sarhan, A. A.; Kuo, T. Y.; Hamdi, M.; Yusof, F.; Chien, C. S.; Ahmed, A.D.; Chang, C. P.; Lee, T. M. *Mater. Chem. Phys.* ***2019, 227***, 358. [Crossref]

[14] Abrosimova, G. E.; Aronin, A. S. *J. Surf. Invest.: X-Ray, Synchrotron Neutron Tech.* **2018**, *2*, 492. [Crossref]

[15] Taghvaei, A. H.; Stoica, M.; Khoshkhoo, M. S.; Thomas, J.; Vaughan, G.; Janghorban, K.; Eckert, J. *Mater. Chem. Phys.* **2012**, *134*, 1214. [Crossref]

[16] Peng, K.; Tang, L.; Wu, Y. *J. Magn. Magn. Mater.* **2018**, *460*, 297. [Crossref]

[17] Li, X.; Wu, Y.; Yang, S.; Cha, X.; Shao, P.; Wang, L. *J. Non-Cryst. Solids* **2019**, *503*, 284. [Crossref]

[18] Masood, A.; Baghbaderanni, H. A.; Strom, V.; Stamenov, P.; Mccloskey, P.; Mathúna, C. Ó.; Kulkarni, S. *J. Magn. Magn. Mater.* **2019**, *483*, 54. [Crossref]

[19] Zhu, M.; Zhang, M.; Yao, L.; Nan, R.; Jian, Z.; Chang, F. E. *Vacuum* **2019**, *163*, 368. [Crossref]

[20] Fang, Y. N.; Hahn, H.; Kobes, S.; Witte, R.; Singh, S. P.; Feng, T.; Ghafari, M. ***Scientific Reports 2019,*** **9**, 1. [Crossref]

[21] Gao, X.; Zhou, Y.; Cheng, Z.; Tan, Y.; Liu, S.; Shen, Z. *Int. J. Hydrogen Energy* **2019**, *44*, 27421. [Crossref]

[22] Nascimento, L.; Costa, A. C. F. M. *Braz. J. Phys.* **2023**, *53*, 158. [Crossref]

How to cite this article

Nascimento, L.; Souza, J. W. L.; Silva, S. M. L.; de Melo Costa, C. F. *Orbital: Electronic J. Chem.* **2025**, *17*, 306. DOI: http://dx.doi.org/10.17807/orbital.v17i4.16546